Inorg. Chem. **2006**, *45*, 7722–7735

Tuning of Inter- versus Intrachain Magnetic Interactions in Cyano-Bridged Ni^{II}/M^{III} (M = Cr, Fe, Co) Chain Complexes

Mihail Atanasov,[†,‡] Peter Comba,*[,†] Sebastian Förster,[†] Gerald Linti,[†] Thomas Malcherek,[§] Ronald Miletich,[§] Alexander I. Prikhod'ko,[†] and Hubert Wadepohl[†]

Universität Heidelberg, Anorganisch-Chemisches Institut, Im Neuenheimer Feld 270, D-69120 Heidelberg, Germany, Insitute of General and Inorganic Chemistry, Bulgarian Academy of Science B1.11, 1113 Sofia, Bulgaria, and Universität Heidelberg, Mineralogisches Institut, Im Neuenheimer Feld 236, D-69120 Heidelberg, Germany

Received March 16, 2006

The reaction of $[M(CN)_6]^{3-}$ (M = Cr^{3+}, Fe^{3+}, Co^{3+}) with the nickel(II) complex of 2,4-diamino-1,3,5-triazin-6-yl-{3-(1,3,5,8,12-pentaazacyclotetradecane)} ($[NiL]^{2+}$) in excess of ANO_3 or ACl (A = Li^+, Na^+, K^+, Rb^+, Cs^+, NH_4^+) leads to the cyano-bridged dinuclear assemblies $A\{[NiL][M(CN)_6]\}\cdot xH_2O$ (x = 2–5). X-ray structures of $Li\{[NiL][Cr(CN)_6]\}\cdot 5H_2O$, $NH_4\{[NiL][Cr(CN)_6]\}\cdot 3.5H_2O$, $K\{[NiL][Cr(CN)_6]\}\cdot 4H_2O$, $K\{[NiL][Fe(CN)_6]\}\cdot 4H_2O$, $Rb\{[NiL][Fe(CN)_6]\}\cdot 3.5H_2O$, and $Cs\{[NiL][Fe(CN)_6]\}\cdot 3.5H_2O$, as well as the powder diffractometry of the entire Fe^{III} series, are reported. The magnetic properties of the assemblies are dependent on the monocation A and discussed in detail. New efficient pathways for ferromagnetic exchange between Ni^{II} and Fe^{III} or Cr^{III} are demonstrated. Field dependencies of the magnetization for the Fe^{III} samples at low temperature and low magnetic field indicate a weak interchain antiferromagnetic coupling, which is switched to ferromagnetic coupling at increasing magnetic field (metamagnetic behavior). The interchain magnetic coupling can be tuned by the size of the A cations.

Introduction

The assembly of crystals from molecular building blocks is an emerging synthetic approach in inorganic materials chemistry. The properties of the resulting materials are predetermined by the nature of the molecular building blocks, as well as their relative orientation in the crystal lattice and the interactions (nonbonded, i.e., electrostatics, H-bonding, van der Waals or bonding) between the molecular building blocks. In the classical example of "prussian blue"-type magnetic materials it has been possible to predict the electronic exchange pathways and magnetic properties by a simple electronic model, which involves two metal centers, bridged by a μ-cyanide ligand.[1,2] However, in general, the effects of relatively weak interactions in the crystal lattice, such as electrostatic interactions, weak coordinative bonds, hydrogen bonding, and van der Waals interactions, and the corresponding structures of the assemblies are difficult to predict.

Heteropolymetalates of transition metals with open d shells and their magnetic properties have been intensively studied for more than two decades.[3,4] Of particular interest are bimetallic cyanide-bridged systems, built from transition metal complex precursors $[M(CN)_6]^{n-}$ and $[M'(OH_2)_6]^{m+}$, with three-dimensional prussian blue-type structures[5] and magnetic ordering below T_c as high as 315 K.[6−9] Photomagnetic behavior of the cyanide complexes has also been reported.[10,11] The magnetism of molecular assemblies is

* To whom correspondence should be addressed. Fax: +49-6221-546617. E-mail: peter.comba@aci.uni-heidelberg.de.
† Universität Heidelberg, Anorganisch-Chemisches Institut.
‡ Insitute of General and Inorganic Chemistry, Bulgarian Academy of Science B1.11.
§ Universität Heidelberg, Mineralogisches Institut.

(1) Guedel, H. U.; Weihe, H. *Comments Inorg. Chem.* **2000**, *22*, 75.
(2) Ruiz, E.; Rodriguez-Fortea, A.; Alvarez, S.; Verdaguer, M. *Chem.—Eur. J.* **2005**, *11*, 2135.
(3) Kahn, O. *Struct. Bonding* **1988**, *68*, 89.
(4) Kahn, O. *Adv. Inorg. Chem.* **1999**, *43*, 179.
(5) Ludi, A. *Struct. Bonding* **1973**, *14*, 1.
(6) Gadet, V.; Mallah, T.; Castro, I.; Veillet, P.; Verdaguer, M. *J. Am. Chem. Soc.* **1992**, *114*, 9213.
(7) Mallah, T.; Thiébaut, S.; Verdaguer, M.; Veillet, P. *Science* **1993**, *262*, 1554.
(8) Entley, W. R.; Girolami, G. S. *Science* **1995**, *268*, 397.
(9) Ferlay, S.; Mallah, T.; Ouahes, R.; Veillet, P.; Verdaguer, M. *Nature* **1995**, *378*, 701.
(10) Sato, O.; Einaga, Y.; Fujishima, A.; Hashimoto, K. *Inorg. Chem.* **1999**, *38*, 4405.
(11) Herrera, J. M.; Marvaud, V.; Verdaguer, M.; Marrot, J.; Kalisz, M.; Mathonière, C. *Angew. Chem., Int. Ed. Engl.* **2004**, *43*, 5468.

10.1021/ic060453q CCC: $33.50
Published on Web 08/23/2006

Scheme 1

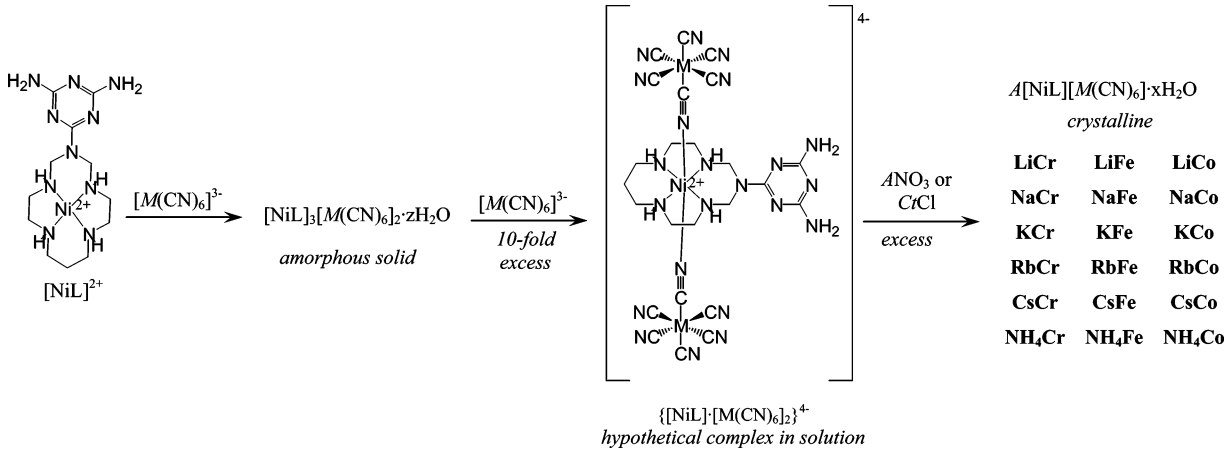

strongly affected by their dimensionality.[12] One approach toward controlled nuclearity in cyanometalates is to use multidentate capping ligands to inhibit the growth of an extended solid and direct the structure of the product.[13] Cyanometalates obtained by this approach include magnetic materials with 3d,[14] pseudo-2d (layers),[15−19] and pseudo-1d structures (chains),[20−39] as well as large-spin single-molecule compounds,[40−53] including single-molecule magnets.[54−66] Hydrothermal syntheses used to prepare cyano-bridged Co(II)−Ni(II) 2d and 1d assemblies with unusual bridging geometries have also been reported.[67]

In this publication, we discuss the structural and electronic/magnetic properties of a cyano-bridged system of chains, based on the nickel(II) macrocyclic ligand complex $[NiL]^{2+}$ (L = 2,4-diamino-1,3,5-triazin-6-yl-{3-(1,3,5,8,12-pentaazacyclotetradecane)}, see Scheme 1) and hexacyanometalates ($M = Fe^{3+}$, Cr^{3+}, Co^{3+}). Variation of the A monocations, which are used for charge neutralization, does not lead to changes in the over-all geometry of the {M−CN−Ni(L)} building blocks. However, there is a variation of the interchain magnetic interactions, resulting from monocations A, which primarily is caused by the size of the A cations.

Results and Discussion

Syntheses and Spectroscopic Properties. The addition of $[M(CN)_6]^{3-}$ to an aqueous solution of $[NiL]^{2+}$ in a ratio of up to 2:3 leads to the formation of amorphous precipitates. These are soluble in an excess of the corresponding cyanometalate, and these solutions probably contain charged complexes (such as $\{[NiL]\cdot[M(CN)_6]_2\}^{4-}$, see Scheme 1). These trinuclear $\{[NiL]\cdot[M(CN)_6]_2\}^{4-}$ complexes form with cations (e.g., K^+ or NH_4^+) insoluble, neutral molecular aggregates. Here, we present our results of the materials crystallized with the monocations $A = Li^+$, Na^+, K^+, Rb^+, Cs^+, and NH_4^+. The combination of three cyanometalates $[M(CN)_6]^{3-}$ ($M = Cr^{3+}$, Fe^{3+}, Co^{3+}) and six A cations results in 18 materials of the general composition $A[NiL][M(CN)_6]\cdot xH_2O$ ($x = 2-5$). We use an abbreviated nomenclature, which specifies the cation A and the metal center M of the cyanometalate (e.g., **NaCr** instead of **Na**[NiL][**Cr**$(CN)_6$]·$5H_2O$).

All compounds described are, after their assembly and crystallization, insoluble in water and common organic

(12) Kahn, O. *Molecular Magnetism*; Wiley & Sons Inc.: New York, 1993.
(13) Mallah, T. In *Localized and Itinerant Molecular Magnetism. From Molecular Assemblies to Devices*; Coronado, E., P. D., Gatteschi, D., Miller, J. S., Eds.; Kluwer: Dordrecht, The Netherlands, 1996; p 576.
(14) Fukita, N.; Ohba, M.; Ōkawa, H.; Matsuda, K.; Iwamura, H. *Inorg. Chem.* **1998**, *37*, 842.
(15) Ferlay, S.; Mallah, T.; Vaissermann, J.; Bartolomé, F.; Veillet, P.; Verdaguer, M. *J. Chem. Soc., Chem. Commun.* **1996**, 2481.
(16) Ohba, M.; Ōkawa, H.; Fukita, N.; Hashimoto, Y. *J. Am. Chem. Soc.* **1997**, *119*, 1011.
(17) Re, N.; Crescenzi, R.; Floriani, C.; Miyasaka, H.; Matsumoto, N. *Inorg. Chem.* **1998**, *37*, 2717.
(18) Marvilliers, A.; Parsons, S.; Rivière, E.; Audière, J.-P.; Kurmoo, M.; Mallah, T. *Eur. J. Inorg. Chem.* **2001**, 1287.
(19) Coronado, E.; Gómez-García, C. J.; Nuez, A.; Romero, F. M.; Waerenborgh, J. C. *Chem. Mater.* **2006**, *18*, 2670.
(20) Ohba, M.; Maruono, N.; Ōkawa, H.; Enoki, T.; Latour, J.-M. *J. Am. Chem. Soc.* **1994**, *116*, 11566.
(21) Ohba, M.; Ōkawa, H.; Ito, T.; Ohto, A. *J. Chem. Soc., Chem. Commun.* **1995**, 1545.
(22) Miyasaka, H.; Matsumoto, N.; Ōkawa, H.; Re, N.; Gallo, E.; Floriani, C. *Angew. Chem.* **1995**, *107*, 1565.
(23) Miyasaka, H.; Matsumoto, N.; Ōkawa, H.; Re, N.; Gallo, E.; Floriani, C. *J. Am. Chem. Soc.* **1996**, *118*, 981.
(24) Ohba, M.; Usuki, N.; Fukita, N.; Ōkawa, H. *Inorg. Chem.* **1998**, *37*, 3349.
(25) Kou, H.-Z.; Zhou, B. C.; Liao, D.-Z.; Wang, R.-J.; Li, Y. *Inorg. Chem.* **2002**, *41*, 6887.
(26) Clérac, R.; Miyasaka, H.; Yamashita, M.; Coulon, C. *J. Am. Chem. Soc.* **2002**, *124*, 12837.
(27) Lescouëzec, R.; Vaissermann, J.; Ruiz-Pérez, C.; Lloret, F.; Carrasco, R.; Julve, M.; Verdaguer, M.; Dromzee, Y.; Gatteschi, D.; Wernsdorfer, W. *Angew. Chem.* **2003**, *115*, 1521.
(28) Colacio, E.; Domínguez-Vera, J. M.; Lloret, F.; Rodríguez, A.; Stoeckli-Evans, H. *Inorg. Chem.* **2003**, *42*, 6962.
(29) Koo, J.; Kim, D.; Kim, Y.-S.; Do, Y. *Inorg. Chem.* **2003**, *42*, 2983.
(30) Lescouëzec, R.; Vaissermann, J.; Toma, L. M.; Carrasco, R.; Lloret, F.; Julve, M. *Inorg. Chem.* **2004**, *43*, 2234.
(31) Toma, L.; Lescouëzec, R.; Vaissermann, J.; Delgado, F. S.; Ruiz-Pérez, C.; Carrasco, R.; Cano, J.; Lloret, F.; Julve, M. *Chem.—Eur. J.* **2004**, *10*, 6130.
(32) Saha, M. K.; Lloret, F.; Bernal, I. *Inorg. Chem.* **2004**, *43*, 1969.
(33) Zhang, Y.-Z.; Gao, S.; Wang, Z.-M.; Su, G.; Sun, H.-L.; Pan, F. *Inorg. Chem.* **2005**, *44*, 4534.
(34) Yoon, J. H.; Kim, H. C.; Hong, C. S. *Inorg. Chem.* **2005**, *44*, 7714.
(35) Toma, L.; Lescouoëzec, R.; Vaissermann, J.; Herson, P.; Marvaud, V.; Lloret, F.; Julve, M. *New J. Chem.* **2005**, *29*, 210.
(36) Lescouëzec, R.; Toma, L. M.; Vaissermann, J.; Verdaguer, M.; Delgado, F. S.; Ruiz-Pérez, C.; Lloret, F.; Julve, M. *Coord. Chem. Rev.* **2005**, *249*, 2691.
(37) Toma, L. M.; Lescouëzec, R.; Pasán, J.; Ruiz-Pérez, C.; Vaissermann, J.; Cano, J.; Carrasco, R.; Wernsdorfer, W.; Lloret, F.; Julve, M. *J. Am. Chem. Soc.* **2006**, *128*, 4842.
(38) Wen, H.-R.; Wang, C.-F.; Zuo, J.-L.; Song, Y.; Zeng, X.-R.; You, X.-Z. *Inorg. Chem.* **2006**, *45*, 582.
(39) Li, D.; Parkin, S.; Wang, G.; Yee, G. T.; Holmes, S. M. *Inorg. Chem.* **2006**, *45*, 1951.

solvents. Therefore, specific procedures were necessary to obtain crystalline samples of all 18 complexes. The final crystalline precipitates were investigated under a microscope and by X-ray powder diffraction (vide infra). The concentration of the initial compounds was varied, and various methods of crystallization were tested. However, for **NaCr** and **NaFe**, only samples of poor crystallinity were obtained. In general, the best results were achieved when the molar ratios of $[NiL]^{2+}/[M(CN)_6]^{3-}$ in solution approached 1:10. With **LiCr**, two types of crystals with different shapes (needles and blocks) cocrystallized. Samples of **NH_4Fe** were isolated as a mixture of a brown and an olive compound, but only the brown crystals could be used for further investigations. The solubility of $RbNO_3$ and $CsNO_3$ was too low to obtain acceptable yields of the assemblies. Therefore, the corresponding chloride salts were used.

Vibrational spectra of all samples have features, which are characteristic for the macrocyclic ligand[68] and the cyanometalate cores:[69] (i) a group of transitions in the range of 1700−1550 cm^{-1} corresponds to the out-of-plane vibrations $\delta(NH_2)$ of the aromatic amino groups of the triazine substituent and ν(NCN) vibrations of the triazine ring, and (ii) vibrations in the range of 2156−2112 cm^{-1} for **AFe**, 2162−2124 cm^{-1} for **ACr**, and 2172−2123 cm^{-1} for **ACo** are assigned to the CN ligands (see Figure S1 and Table S1, Supporting Information). As has previously been shown, vibrations of the μ-bridging CN ligands (ν_{bridge}) appear at ∼20−30 cm^{-1} higher in energy than the vibrations of terminal CN donors ($\nu_{terminal.}$)[70,71] (Table S1, Figure S1b). This effect is attributed to the stabilization of the doubly occupied σ(2s) antibonding orbital of the bridging CN ligand through overlap with the M orbitals, which strengthens the CN bond. In most of the spectra, there are two transitions for the bridging CN groups (Table S1), resulting from the coordination of the CN groups to nickel(II) and a reduction of the symmetry by coordination to the A cations (see structural section below); the CN vibrations of the hexacyanometalates appear as single bands at 2118 (Fe^{3+}), 2128 (Cr^{3+}), and 2129 (Co^{3+}) cm^{-1}.[69] Traces of iron(II) (low-intensity band at about 2030 (Figure S1b) vs 2040 cm^{-1} in $[Fe(CN)_6]^{4-}$ [69]) were found in all samples obtained from $[Fe(CN)_6]^{3-}$; this indicates a slow reduction of iron(III) under the synthetic conditions.

Details of the X-ray powder diffraction patterns of the polycrystalline **AFe** samples are shown in Figure 1. The structural similarity of the **KFe**, **RbFe**, and **CsFe** complexes is evident, as the peak positions agree with those obtained by independent full profile fits of the **KFe** diffraction data (SG symmetry *Pbca*). The peak positions of **LiFe** correspond to the smaller cell found for the **LiCr** compound by single-crystal diffraction (SG symmetry $Pca2_1$, Table 5). Refined lattice parameters are $a = 26.021(3)$ Å, $b = 10.302(1)$ Å, and $c = 11.777(1)$ Å. The powder diffraction data for **NaFe** indicate the presence of both phases. The powder diffraction patterns of the K, Rb, and Cs complexes also show some evidence for the coexistence of minor amounts of the $Pca2_1$ phase, as indicated by the presence of a weak 201 peak, which is symmetry forbidden in the *Pbca* phase.

Molecular and Crystal Structures. Except for **LiCr, LiFe**, and **NaFe**, all complexes crystallize in the orthorhombic spacegroup *Pbca* with two formula units in the asymmetric unit. Complex **LiCr** (spacegroup $Pca2_1$, racemic twin) has only one formula unit in the asymmetric unit, resulting in the unit cell volume being approximately a quarter of that for the other complexes. Despite this difference, the gross structures of the polyanionic backbones of all the complexes are quite similar (see Figure 2 for plots of the molecular subunits). There are chains of $[-NC-M(CN)_4-CN-Ni(macrocycle)-]_n$ units (M = Fe or Cr) running parallel to one of the crystal axes (the direction normal to the *a* glide, i.e., crystal *b* in **LiCr** and crystal *c* in all others). Some direct

(40) Mallah, T.; Auberger, C.; Verdaguer, M.; Veillet, P. *J. Chem. Soc., Chem. Commun.* **1995**, 61.
(41) Larionova, J.; Gross, M.; Pilkington, M.; Andres, H.; Stoeckli-Evans, H.; Güdel, H. U.; Decurtins, S. *Angew. Chem.* **2000**, *112*, 1667.
(42) Oshio, H.; Tamada, O.; Onodera, H.; Ito, T.; Ikoma, T.; Tero-Kubota, S. *Inorg. Chem.* **1999**, *38*, 5686.
(43) Berseth, P. A.; Sokol, J. J.; Shores, M. P.; Heinrich, J. L.; Long, J. R. *J. Am. Chem. Soc.* **2000**, *122*, 9655.
(44) Zhong, Z. J.; Seino, H.; Mizobe, Y.; Hidai, M.; Fujishima, A.; Ohkoshi, S.; Hashimoto, K. *J. Am. Chem. Soc.* **2000**, *122*, 2952.
(45) Oshio, H.; Yamamoto, M.; Ito, T. *Inorg. Chem.* **2002**, *41*, 5817.
(46) Yang, J. Y.; Shores, M. P.; Sokol, J. J.; Long, J. R. *Inorg. Chem.* **2003**, *42*, 1403.
(47) Berlinguette, C. P.; Galán-Mascarós, J. R.; Dunbar, K. R. *Inorg. Chem.* **2003**, *42*, 3416.
(48) Marvaud, V.; Decroix, C.; Scuiller, A.; Tuyèras, F.; Guyard-Duhayon, C.; Vaissermann, J.; Marrot, J.; Gonnet, F.; Verdaguer, M. *Chem.—Eur. J.* **2003**, *9*, 1692.
(49) Marvaud, V.; Decroix, C.; Scuiller, A.; Guyard-Duhayon, C.; Vaissermann, J.; Gonnet, F.; Verdaguer, M. *Chem.—Eur. J.* **2003**, *9*, 1678.
(50) Herchel, R.; Boča, R.; Gembicky, M.; Kož í šek, J.; Renz, F. *Inorg. Chem.* **2004**, *43*, 4103.
(51) Ni, Z.-H.; Kou, H.-Z.; Zhang, L.-F.; Ni, W.-W.; Jiang, Y.-B.; Cui, A.-L.; Ribas, J.; Sato, O. *Inorg. Chem.* **2005**, *44*, 9631.
(52) Rebilly, J.-N.; Catala, L.; Rivière, E.; Guillot, R.; Wernsdorfer, W.; Mallah, T. *J. Chem. Soc., Chem. Commun.* **2006**, 735.
(53) Li, D.; Wang, G.; Yee, G. T.; Holmes, S. M. *Inorg. Chem.* **2006**, *45*, 2773.
(54) Scuiller, A.; Mallah, T.; Verdaguer, M.; Nivorozkhin, A.; Tholence, J.-L.; Veilett, P. *New J. Chem.* **1996**, *20*, 1.
(55) Van Langenberg, K.; Batten, S. R.; Berry, K. J.; Hockless, D. C. R.; Moubaraki, B.; Murray, K. S. *Inorg. Chem.* **1997**, *36*, 5006.
(56) Sokol, J. J.; Hee, A. G.; Long, J. R. *J. Am. Chem. Soc.* **2002**, *124*, 7656.
(57) Berlinguette, C. P.; Vaughn, D.; Cañada-Vilalta, C.; Galán-Mascarós, J. R.; Dunbar, K. R. *Angew. Chem.* **2003**, *115*, 1561.
(58) Wang, S.; Zuo, J.-L.; Zhou, H.-C.; Choi, H. J.; Ke, Y.; Long, J. R.; You, X.-Z. *Angew. Chem., Int. Ed.* **2004**, *43*, 5940.
(59) Choi, H. J.; Sokol, J. J.; Long, J. R. *Inorg. Chem.* **2004**, *43*, 1606.
(60) Miyasaka, H.; Takahashi, H.; Madanbashi, T.; Sugiura, K.; Clérac, R.; Nojiri, H. *Inorg. Chem.* **2005**, *44*, 5969.
(61) Li, D.; Parkin, S.; Wang, G.; Yee, G. T.; Prosvirin, A. V.; Holmes, S. M. *Inorg. Chem.* **2005**, *44*, 4903.
(62) Schelter, E. J.; Prosvirin, A. V.; Dunbar, K. R. *J. Am. Chem. Soc.* **2004**, *126*, 15004.
(63) Song, Y.; Zhang, P.; Ren, X.-M.; Shen, X.-F.; Li, Y.-Z.; You, X.-Z. *J. Am. Chem. Soc.* **2005**, *127*, 3708.
(64) Beltran, L. M. C.; Long, J. R. *Acc. Chem. Res.* **2005**, *38*, 325.
(65) Li, D.; Parkin, S.; Wang, G.; Yee, G. T.; Clérac, R.; Wernsdorfer, W.; Holmes, S. M. *J. Am. Chem. Soc.* **2006**, *128*, 4214.
(66) Wang, C.-F.; Zuo, J.-L.; Bartlett, B. M.; Song, Y.; Long, J. R.; You, X.-Z. *J. Am. Chem. Soc.* **2006**, *128*, 7162.
(67) Rodriguez, A.; Sakiyama, H.; Masciocchi, N.; Galli, S.; Gálvez, N.; Lloret, F.; Colacio, E. *Inorg. Chem.* **2005**, *44*, 8399.
(68) Atanasov, M.; Comba, P.; Lampeka, Y. D.; Linti, G.; Malcherek, T.; Miletich, R.; Prikhod'ko, A. I.; Pritzkow, H. *Chem.—Eur. J.* **2006**, *12*, 737.
(69) Nakamoto, K. *Infrared and Raman Spectra of Inorganic and Coordination Compounds*, 4th ed.; John Wiley & Sons: New York, 1986.
(70) Swanson, B. L. *Inorg. Chem.* **1976**, *15*, 253.
(71) Bernhardt, P. V.; Bozoglian, F.; Macpherson, B. P.; Martinez, M. *J. Chem. Soc., Dalton Trans.* **2004**, 2582.

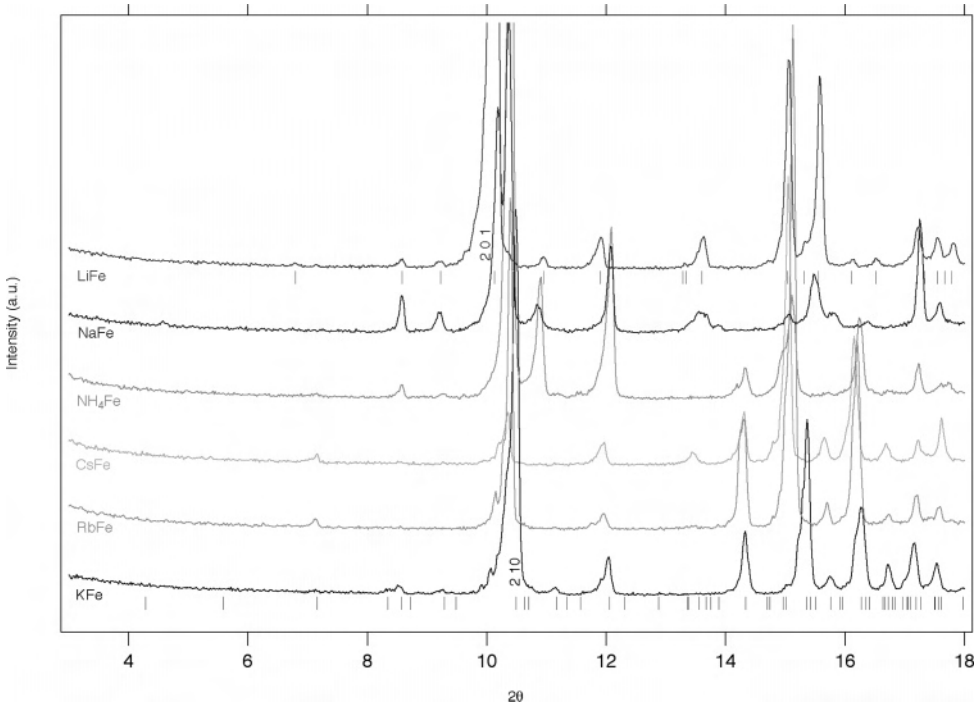

Figure 1. Details of the X-ray powder diffraction patterns of the **AFe** assemblies at small diffraction angles. The lower peak markers refer to the **KFe** sample, and the upper row of peak markers indicate the peak positions for the smaller **LiFe** cell.

hydrogen bonding between the chains is present (the donors are always amino groups of the melamine moiety, and the acceptors are mostly cyanide nitrogens and, in a few cases, also a ring nitrogen of a triazine residue), but linkage of the chains to one another is mainly achieved via the alkaline cations (vide infra).

The interatomic distances and angles of the macrocyclic ligand nickel(II) fragments are almost identical for all structures. They are very similar to published data,[68−72] as expected for the trans-III (RRSS) conformation of a cyclam-derived macrocycle coordinated to nickel(II).[73] The structural parameters of the NiN_6 chromophore (in-plane macrocyclic amines and axial CN bridges) are as expected for pseudo-octahedral nickel(II) geometries: the four amine donors are ∼2.08 Å from the nickel(II) center, and the two axially bridging CN groups are at a distance of ∼2.10 Å (see Table S2). The Ni−N≡C angles deviate from 180° (Table S2), but this is not unusual for cyanometalate assemblies.[1] The $[Cr(CN)_6]^{3-}$ and $[Fe(CN)_6]^{3-}$ fragments are approximately octahedral, with bond lengths and angles as expected[74] (Table S2).

Because of the asymmetry of the substituted pentaazacyclotetradecane ligand, the crystal structures show a distinct aggregation pattern: there are polar areas in the lattices, with the triazine substituents bound to the alkaline cations, as well as nonpolar regions, because of the aliphatic backbone of the macrocyclic ligands. Water is present in the polar regions, either coordinated to the alkali metal cations or as solvent molecules of crystallization (sometimes in only fractionally populated sites). As shown in Figure 3, each cyanide-bridged Ni(II)−M(III) chain has a direction determined by the orientation of the macrocyclic ligand. Adjacent chains with the same directions are connected to give double layers. These connections are formed by hydrogen bonds (vide supra) or by bonds of the A cations to nitrogen donors. This gross packing motif is common to all structures discussed here. As far as the linkage type and geometry are concerned, there are, however, important differences, which are mainly the result of the coordination mode of the singly charged cations.

The lithium ion in **LiCr** is coordinated by three water molecules and one nitrogen atom of a cyanide group of $[Cr(CN)_6]^{3-}$ (see Figure 2 and Table 1), resulting in a distorted tetrahedral coordination geometry (Figure 2a). The macrocyclic ligand complexes do not bind the lithium ions with the triazine residue but support the structure by hydrogen bonds to a coordinated water molecule. The lithium ions are not directly connected to any of the neighboring $[-NC-M(CN)_4-CN-Ni(macrocycle)-]_n$ chains. This structure can therefore be considered to be built of "magnetically isolated" cyano-bridged nickel(II)−chromium(III) chains.

In the other structures, the A cations establish connections between adjacent $[-NC-M(CN)_4-CN-Ni(macrocycle)-]_n$ chains within the double layers. In **NH_4Cr**, there are hydrogen bonds between the ammonium ion and some cyanide ligands (Figure 2b), linking $[Cr(CN)_6]^{3-}$ units from three adjacent chains (Table 1). However, a transfer of magnetic interactions through hydrogen bonds of the am-

(72) Comba, P.; Lampeka, Y. D.; Nazarenko, A. Y.; Prikhod'ko, A. I.; Pritzkow, H.; Taraszewska, J. *Eur. J. Inorg. Chem.* **2002**, 1871.
(73) Boeyens, J. C. A.; Dobson, S. M. Stereochemical and Stereophysical Behaviour of Macrocycles. In *Stereochemical and Stereophysical Behaviour of Macrocycles*; Bernal, I., Ed.; Elsevier: Amsterdam, 1987; p 1.
(74) Orpen, A. G.; Bramner, L.; Allen, F. H.; Kennard, O.; Watson, D. G.; Taylor, R. *J. Chem. Soc., Dalton Trans.* **1989**, 1.

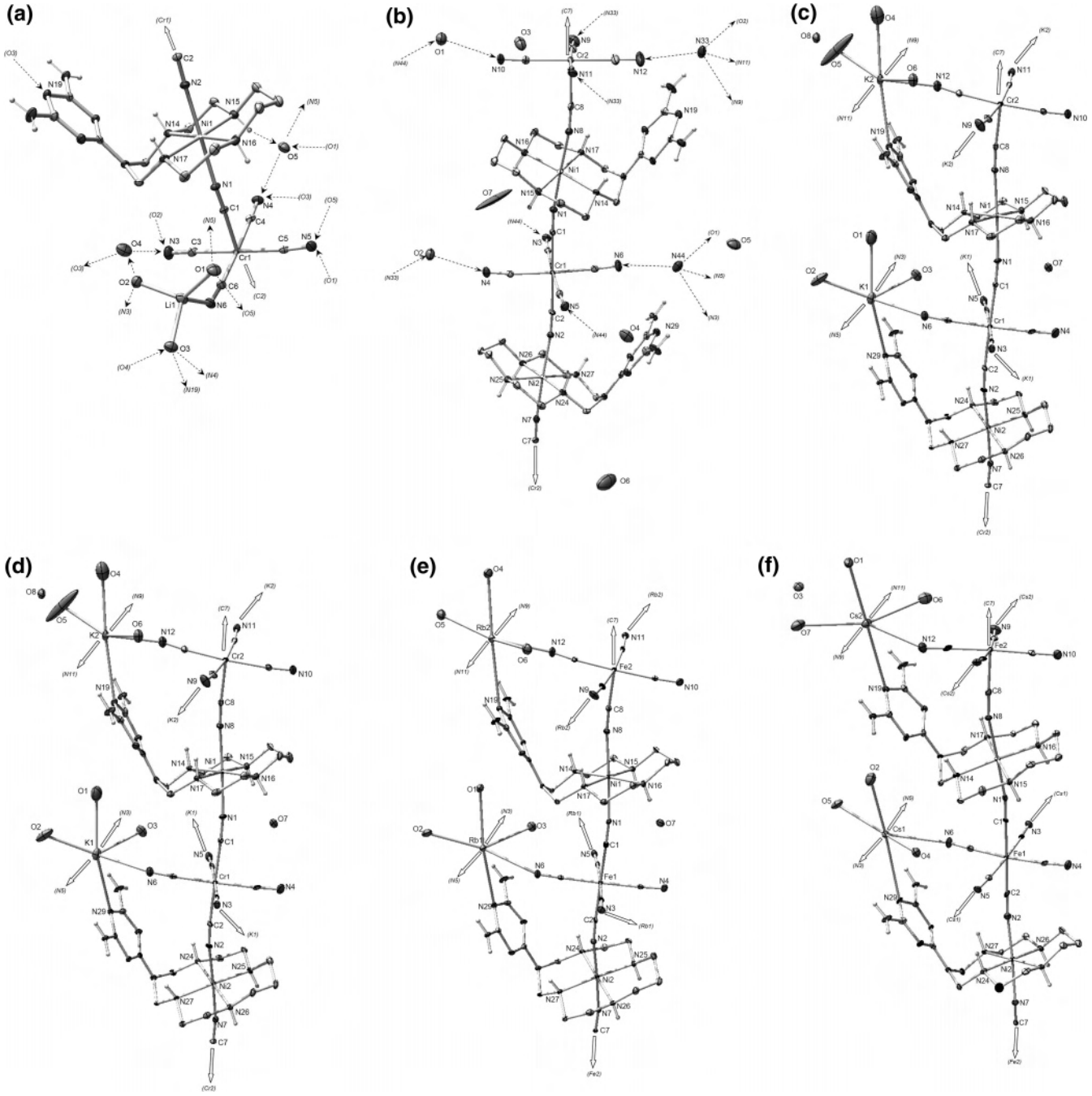

Figure 2. ORTEP plot (30% probability ellipsoids) of the molecular subunits of Li[NiL][Cr(CN)$_6$]·5H$_2$O (**LiCr**) (a), NH$_4$[NiL][Cr(CN)$_6$]·3.5H$_2$O (**NH$_4$Cr**) (b), K[NiL][Cr(CN)$_6$]·4H$_2$O (**KCr**) (c), K[NiL][Fe(CN)$_6$]·4H$_2$O (**KFe**) (d), Rb[NiL][Fe(CN)$_6$]·3.5H$_2$O (**RbFe**) (e), and Cs[NiL][Fe(CN)$_6$]·3.5H$_2$O (**CsFe**) (f). The hydrogen atoms are omitted for clarity, and coordinative and hydrogen bonds are depicted with arrows.

monium ions should be weaker than the more direct interaction via an alkali metal ion. Therefore, this binding mode is considered an intermediate case between the **LiCr** and **KCr** structures (vide infra).

The coordination modes of cation A in the crystals of **KCr**, **KFe**, and **RbFe** are all very similar (Figure 2c−f). In general, A connects three cyano groups from adjacent chains with the CN groups almost in-plane. The coordination sphere of A is completed to seven ligands with three molecules of water and a nitrogen atom from the triazine residue. This coordination mode is shown in Figure 4a, and the corresponding geometric parameters are given in Table 1.

Figure 4 shows that, in **KCr**, **KFe**, **RbFe**, and **CsFe**, each alkali metal ion bridges three cyanometalate units in a direction perpendicular to a $[-NC-M-CN-Ni]_n$ chain, resulting in a 3D-network of cyano-bridged metal ions (Figure 4b). This network, however, is expanded only along the polar area of the structure (see above and Figure 3). The binding mode of the alkali ions provides an additional pathway for magnetic interactions, and in analogy to "spin ladders", the cyano-bridged network may be described as a "double-layered spin wall". Therefore, a continuous and regular change of the magnetic properties of these assemblies is expected, since the interatomic distances, A−NC, increase

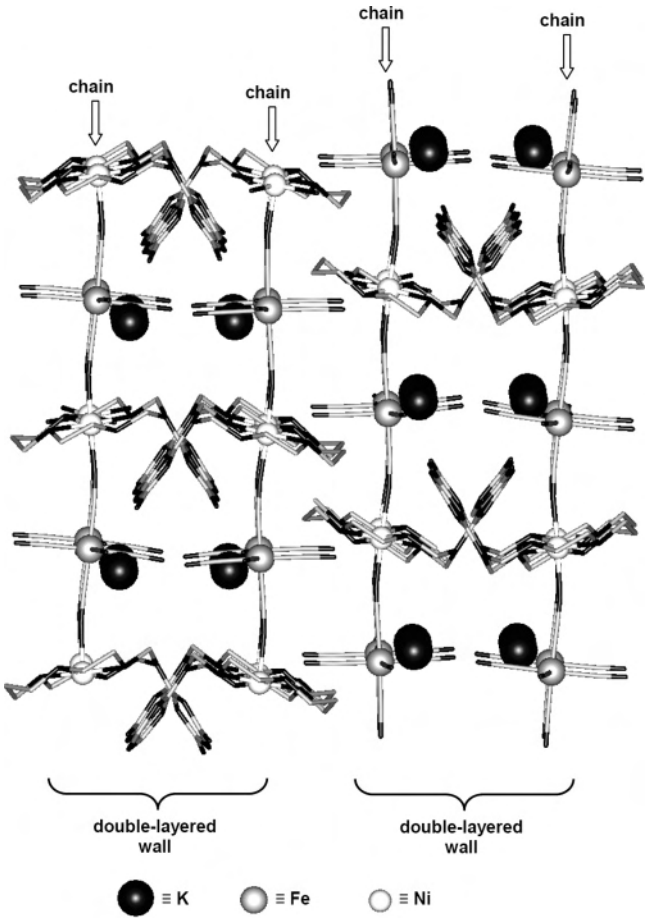

Figure 3. Schematic representation of the crystal structures of the assemblies with the example of **KFe**; the hydrogen atoms and water molecules are omitted for clarity.

regularly in the order K < Rb < Cs (Table 1). The expected change of magnetic properties along the series of materials also emerges from the structural parameters defined in Figure 5 and listed in Table 2. The distances between the chromium(III) or iron(III) centers are significantly shorter for **KCr**, **KFe**, **RbFe**, and **CsFe** than for **LiCr**. This agrees with the expectations based on the molecular structures and supports the assumption that the magnetic behavior of the lithium assemblies might be based on isolated, cyano-bridged nickel(II)−chromium(III) chains, whereas for potassium, rubidium, and cesium, there are interchain pathways for magnetic-exchange interactions.

Electronic Spectra and Magnetic Properties. The magnetic properties of the systems under consideration are determined by the ground states of $[M(CN)_6]^{3-}$ ($M = Cr^{III}$, low-spin Fe^{III}, and Co^{III}), which are $^4A_2$ (Cr^{III}), $^2T_2$(Fe^{III}), and $^1A_1$(Co^{III}), and the $^3A_2$ $[Ni^{II}N_6]$ chromophore. While the electronic spectra and the magnetic behavior of isolated $[M(CN)_6]^{3-}$ are well understood[75] and octahedral hexamine complexes of Ni^{2+} have been known for a long time,[76] little is known about the bonding character of the CN bridging ligands. In particular, the low symmetry of the ligand field in the *trans*-$[Ni(NHR_2)_4(NC)_2]^{2+}$ chromophore might lead to a significant anisotropy and a corresponding zero-field splitting of the $^3A_2$ ground state and to interesting magnetic

Table 1. Interatomic Distances (Å) and Angles (deg) for A and Adjacent Atoms (see Figures 2−4)

	LiCr[a]	NH_4Cr[b]	KCr[c]	KFe[d]	RbFe[e]	CsFe[f]
A1−Z	2.065(7)	3.064(8)	2.862(7)	2.98(2)	2.887(4)	2.983(9)
A1−T	1.904(7)	3.126(9)	3.094(5)	2.972(6)	3.168(5)	3.283(8)
A1−R	1.942(7)	2.969(8)	3.009(5)	3.140(6)	3.290(5)	3.411(7)
A1−D	1.944(7)	2.911(8)	2.803(7)	2.617(8)	2.922(4)	3.074(8)
A1−E			3.008(5)	2.916(6)	3.140(5)	3.281(8)
A1−Q			2.879(5)	2.926(6)	2.995(4)	3.199(7)
A1−G			2.910(6)	2.807(7)	3.040(5)	3.145(8)
Z−A1−R	105.6(3)	131.6(5)	113.4(2)	95.9(4)	112.7(1)	114.8(2)
Z−A1−D	114.6(3)	96.8(5)	68.3(2)	44.8(4)	68.8(1)	68.9(2)
Z−A1−E			90.4(2)	94.0(4)	93.3(1)	93.9(2)
Z−A1−Q			74.9(2)	87.2(4)	82.3(1)	84.3(2)
Z−A1−G			101.4(2)	105.0(4)	109.0(1)	112.2(2)
T−A1−R	124.7(4)	85.1(4)	84.8(1)	84.2(2)	82.2(1)	79.4(2)
T−A1−D	109.5(3)	114.3(5)	126.7(2)	135.92	120.5(1)	118.6(2)
T−A1−E			81.8(1)	86.6(2)	78.0(1)	76.4(2)
T−A1−Q			86.3(1)	92.4(2)	84.4(1)	84.0(2)
T−A1−G			73.8(1)	74.1(2)	70.9(1)	69.9(2)
Z−A1−T	100.7(3)	123.3(5)	160.8(2)	179.1(4)	165.1(1)	165.7(2)
R−A1−D	102.3(3)	105.9(5)	70.4(2)	66.2(2)	67.2(1)	66.3(2)
D−A1−E			79.5(2)	88.5(2)	80.3(1)	79.8(2)
E−A1−Q			78.9(1)	72.9(2)	80.2(1)	82.4(2)
Q−A1−G			65.7(1)	66.5(2)	65.4(1)	65.4(2)
G−A1−R			82.6(1)	90.0(2)	82.2(1)	81.5(2)
A1−N3−C3		139.5(5)	138.4(4)	149.0(5)	137.7(4)	135.9(7)
A1−N5−C5		159.9(5)	164.2(4)	163.0(6)	162.4(4)	158.2(6)
A1−N6−C6	138.3(3)	158.3(5)	153.7(5)	152.3(6)	152.5(4)	149.8(2)

	LiCr	NH_4Cr[g]	KCr[h]	KFe[i]	RbFe[j]	CsFe[k]
A2−Z		3.036(9)	2.854(8)	2.99(4)	2.878(5)	2.999(7)
A2−T		3.010(8)	3.050(5)	2.993(6)	3.167(4)	3.302(7)
A2−R		2.852(8)	3.049(6)	3.050(6)	3.306(5)	3.390(8)
A2−D		2.873(8)	2.52(2), 2.972(8)[l]	2.721(7)	3.028(5)	3.197(9)
A2−E			2.888(5)	3.087(6)	3.012(4)	3.146(7)
A2−Q			2.910(5)	2.847(6)	2.878(5)	3.264(9)
A2−G			2.781(6)	2.910(7)	2.917(5)	3.037(9)
Z−A2−R		106.8(5)	94.2(2)	107.4(3)	95.1(1)	99.3(2)
Z−A2−D		107.2(5)	40.1(3), 69.6(2)[l]	58.6(3)	70.3(1)	71.8(2)
Z−A2−E			97.9(2)	89.7(3)	102.4(1)	103.4(2)
Z−A2−Q			88.2(2)	78.1(3)	94.3(1)	96.4(2)
Z−A2−G			99.5(2)	103.6(4)	105.6(1)	109.5(2)
T−A2−R		110.9(5)	83.6(1)	86.2(2)	80.9(1)	78.0(2)
T−A2−D		99.9(5)	142.0(3), 113.1(2)[l]	131.0(2)	109.6(1)	107.7(2)
T−A2−E			87.3(1)	82.9(2)	82.9(1)	79.8(2)
T−A2−Q			91.5(1)	88.9(2)	87.9(1)	85.2(2)
T−A2−G			75.2(2)	74.7(2)	70.8(1)	68.6(2)
Z−A2−T		124.8(5)	174.4(2)	166.2(3)	174.7(1)	176.7(2)
R−A2−D		105.6(5)	68.0(3), 57.5(2)[l]	69.7(2)	54.5(1)	52.6(2)
D−A2−E			92.8(3), 83.1(2)[l]	81.8(2)	86.7(1)	87.0(2)
E−A2−Q			73.9(1)	77.4(2)	74.1(1)	75.0(2)
Q−A2−G			67.7(2)	66.2(2)	66.9(1)	65.8(2)
G−A2−R			86.3(2)	84.8(2)	85.8(1)	86.7(2)
A2−N9−C9		149.1(5)	164.1(5)	168.6(5)[i]	161.2(4)	156.0(7)
A2−N11−C11		160.3(5)	149.1(5)	137.2(5)	150.2(4)	148.8(7)
A2−N12−C12		174.3(5)	147.3(5)	154.1(5)	150.3(4)	148.8(7)

[a] A1 = Li1, Z = N6, T = O1, R = O2, D = O3. [b] A1 = N44, Z = N3, T = N5, R = N6, D = O1. [c] A1 = K1, Z = O1, T = N29, R = N5, D = O2, E = N3, Q = O3, G = N6, [d] A1 = K1, Z = O3, T = N29, R = N5, D = O2, E = N3, Q = O1, G = N6. [e] A1 = Rb1, Z = O1, T = N29, R = N5, D = O2, E = N3, Q = O3, G = N6. [f] A1 = Cs1, Z = O2, T = N29, R = N5, D = O5, E = N3, Q = O4, G = N6. [g] A2 = N33, Z = N9, T = N11, R = N12, D = O2. [h] A2 = K2, Z = O4, T = N19, R = N9, D = O5, E = N11, Q = O6, G = N12. [i] A2 = K2, Z = O5, T = N19, R = N10, D = O6, E = N11, Q = O4, G = N12; c1 N9 = N10, C9 = C10.[j] A2 = Rb2, Z = O4, T = N19, R = N9, D = O5, E = N11, Q = O6, G = N12. [k] A2 = Cs2, Z = O1, T = N19, R = N9, D = O7, E = N11, Q = O6, G = N12. [l] Two disordered positions.

(75) Alexander, J. J.; Gray, H. B. *J. Am. Chem. Soc.* **1968**, *90*, 4260.
(76) Jorgensen, C. K. *Absorption Spectra and Chemical Bonding in Complexes;* Pergamon Press: Oxford, U.K., 1962.

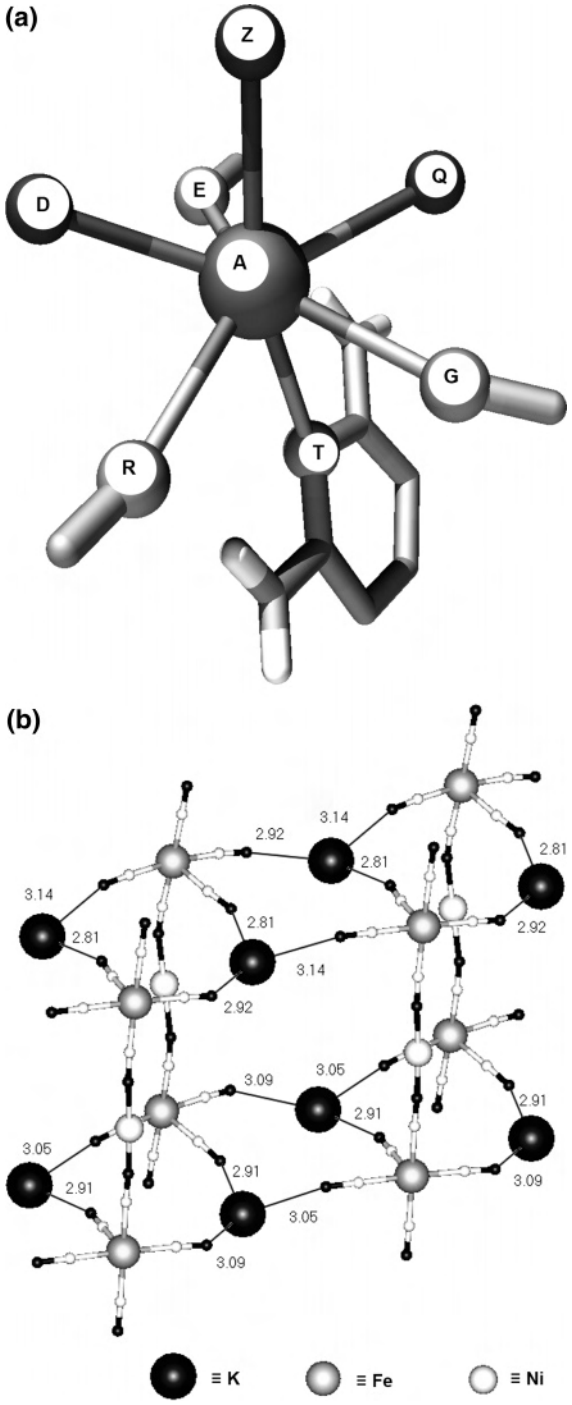

Figure 4. Schematic presentation of the bridging mode of the singly charged cation in **KCr**, **KFe**, **RbFe**, and **CsFe** (a) and the network of metal ions in **KFe** connected by cyanide bridges (b). The K−N interatomic distances (Å) are shown in part b; macrocyclic ligands, water molecules, and nonbridging cyanides are omitted for clarity.

properties. Therefore, we have recorded the ligand-field spectra of the **KM** complexes (M = Co^{III}, Fe^{III}, and Cr^{III}, see Figure 6). The spectra of the three complexes are characterized by a broad absorption band between 10 000 and 15 000 cm^{-1}, which we identify as the $^3A_2 \rightarrow {}^3T_2$ transition of $[NiN_6]$. Higher-energy transitions within the same chromophore are obscured by d−d excitations and CT transitions of $[Cr(CN)_6]^{3-}$ and $[Fe(CN)_6]^{3-}$, respectively. These shift to higher energies for **KCo** (d−d absorptions of

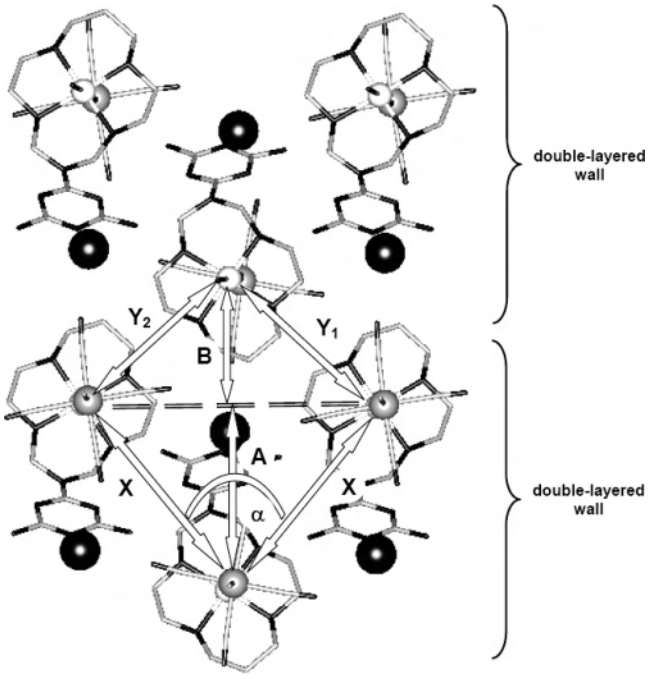

Figure 5. Schematic representation of the crystal structures; the hydrogen atoms and water molecules are omitted for clarity.

Table 2. Structural Parameters of the Crystal Structures in Dependence of the Singly Charged Cations A

	LiCr	NH_4Cr	KCr	KFe	RbFe	CsFe
X	9.74	9.34	9.22	9.13	9.29	9.44
Y_1	7.87	7.94	7.98	7.74	7.88	7.91
Y_2	7.68	7.30	7.44	7.63	7.37	7.35
α	74.7	77.4	78.7	78.3	78.6	77.0
A	7.74	7.29	7.13	7.08	7.19	7.39
B	5.05	4.89	5.02	5.08	4.84	4.86
*X**		9.31	9.21	9.11	9.23	9.38
Y_1*		7.84	7.77	7.90	7.73	7.78
Y_2*		7.49	7.69	7.49	7.64	7.62
α*		77.8	78.7	78.5	78.1	77.6
*A**		7.25	7.12	7.06	7.17	7.31
*B**		4.95	5.06	5.09	5.02	4.97
$\bar{A}$	7.74	7.27	7.13	7.07	7.18	7.35
$\bar{B}$	5.05	4.92	5.04	5.09	4.93	4.92

$Co(CN)_6^{3-}$ are known to appear above 30 000 cm^{-1}).[76] The spectrum of **KCo** allows the identification of four spin-allowed $[NiN_6]$ d−d transitions (11500, 14 000, 17 500, and

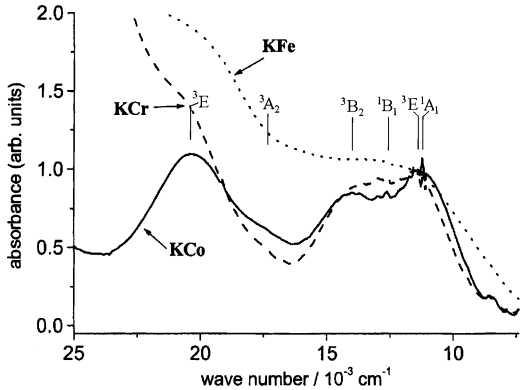

Figure 6. Room temperature UV−vis diffused reflectance spectra of **KCo** (—), **KCr** (- - -), and **KFe** (···). Assignments of the spectral band maxima from the d−d transitions within the $[Ni(NHR_2)_4(NC)_2]^{2+}$ chromophores are based on calculations using the angular overlap model.

Table 3. Multiplet Energies (in cm^{-1}) of the *trans*-$[Ni(NR_3)_4(NC)_2]^{2+}$ Chromophore, Calculated Using the Angular Overlap Model and Ligand-Field Parameters Deduced from a Fit to the Observed Spectral d−d Transitions (Figure 6)[a]

electronic state		energy ($\zeta = 0$)		electronic state	energy ($\zeta^c = 470$)
O	D_4	calcd	exptl	D_4*	calcd
$^3A_2$	$^3B_1$	0		Γ_4	0
				Γ_5	2.63
$^3T_2$	^3E	11 347	11 500	Γ_2	11 150
				Γ_3	11 367
				Γ_5	11 376
				Γ_1	11 548
				Γ_4	11 610
	$^3B_2$	14 340	14 000	Γ_5	14 358
				Γ_3	14 408
$^3T_1$	$^3A_2$	17 786	≅17 500	Γ_5	17 819
				Γ_1	17 824
	^3E	20 094	20 500	Γ_1	19 977
				Γ_2	20 061
				Γ_5	20 170
				Γ_4	20 227
				Γ_3	20 298
^1E	$^1A_1$	11 072	11 250	Γ_1	10 625
	$^1B_1$	12 276	12 500	Γ_3	12 413
e_σ(eq)[b]				4780	
e_σ(ax)[b]				2950	
B				785	

[a] $C/B = 4$. [b] e_π parameters for Ni−N_{amine} and Ni−$N_{isocyano}$ bonds have been fixed at zero. [c] Adopted value of the spin−orbit constant is that of the free Ni^{2+} ion (ζ_o= 649 cm^{-1}) reduced by 25% because of covalency (ζ = 470 cm^{-1}).

20 500 cm^{-1}). In addition, two sharp peaks at 11 250 and 12 500 cm^{-1}, from spin-forbidden electronic excitations, are observed. These gain intensity from the spin-allowed transition via spin−orbit coupling, which is rather pronounced in the case of Ni^{2+}. An interpretation with the angular overlap model was possible, which is compatible with the observed intensity distribution (Figure 6). With this assignment, the tetragonal splitting of the $^3T_2$ and $^3T_1$ excited states and the angular overlap parameters have been deduced (see Table 3). From the calculated bonding parameters, a clear bonding anisotropy with stronger equatorial Ni−N_{amine} (e_σ(eq) = 4780 cm^{-1}) and weaker axial Ni−N_{NC} (e_σ(ax) = 2950 cm^{-1}) ligand fields is found. This leads, after introduction of spin−orbit coupling, to a significant $^3A_2$ (positive) zero-field splitting (2.63 cm^{-1}), with the $M_s = 0$ (Γ_4) split state below $M_s = \pm 1$ (Γ_5).

Temperature-dependent molar magnetic susceptibilities (χ) and field dependencies of the magnetization (M) of **KCr**, **KFe**, and **KCo** were measured in the temperature range of 2−300 K. Figures 7 and 8 show the corresponding χT versus T and M versus B plots. Room-temperature data for χT (B = 1 kG) and the magnetization, M (B = 50 kG, T = 1.8 K), together with the calculated values of these quantities, based on spin-only formulas for noninteracting spin momenta (room-temperature data), are listed in Table 4. There is good agreement between the total number of spins and the experiment. However, the orbital contributions from spin−orbit coupling are found to be important in all complexes. These lead to positive deviations of the room-temperature χT data, compared with their spin-only values, and this is

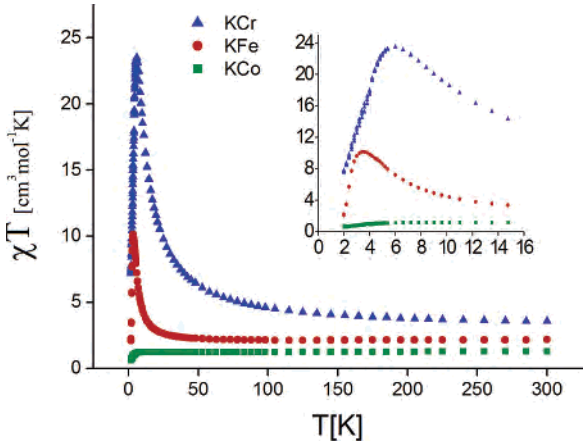

Figure 7. Plots of χT vs T for **KCr**, **KFe**, and **KCo**.

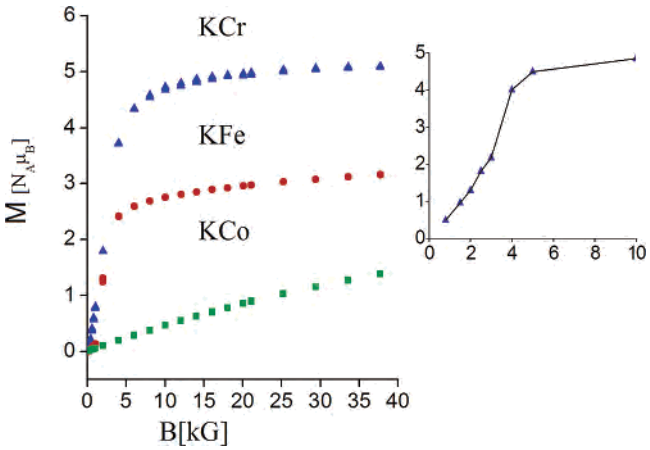

Figure 8. Field (B) dependencies (T = 1.8 K) of the magnetization M for **KCr**, **KFe**, and **KCo**.

Table 4. Magnetic Data of the Cyanometalate KM (M = Co^{III}, Fe^{III}, Cr^{III}) Complexes

	χT (cm^3 mol^{-1} K) (T = 298 K, B = 1 kG)		M ($N_A\mu_B$) (T = 1.8 K, B = 50 kG)	
	exptl	calcd (g_e = 2.00)	exptl	calcd (g_e = 2.00)
KCo	1.28	1.00	1.70	2.00
KFe	2.17	1.38	3.25	3.00
KCr	3.56	2.88	5.12	5.00

particularly pronounced in the case of $[Fe(CN)_6]^{3-}$, with an orbitally degenerate ground state (see below). As expected, on the basis of the nonoverlapping $e_g(\sigma)$ and $t_{2g}(\pi)$ magnetic orbitals of $[NiN_6]$ and $[Fe(CN)_6]^{3-}$ or $[Cr(CN)_6]^{3-}$, respectively, there is a ferromagnetic coupling between the Ni−Fe and Ni−Cr pairs. This is manifested by the increase of the χT versus T curves toward lower temperatures and above critical values of 30 K (**KFe** for the Ni−Fe pair) and 70 K (**KCr** for the Ni−Cr pair), followed by a drop of χT below the temperature of the maxima at about 6 K for **KCr** and 2.5 K for **KFe** (see Figure 7). Such a behavior is typical for magnetic chain compounds with ferro- or ferrimagnetic intrachain coupling and is usually attributed to interchain antiferromagnetic coupling.[35] However, in the present cases, single-ion anisotropy of Ni^{2+} might be responsible for this

behavior (nonmagnetic $M_s = 0$ ground state for $T = 0$). In support of this, we note that the temperature of the maximum in the χT versus T curves (2.0−3.5 cm^{-1}) is of a comparable size with the zero-field splitting parameter of Ni^{2+}, deduced from the electronic spectra ($D = 2.7$ cm^{-1}, vide supra). This might also be responsible for the lowering of χT below the same temperature for the paramagnetic **KCo** material (see Figure 7), which has a $^1A_1$ ground state on Co. However, a weak interchain antiferromagnetic coupling involving Fe^{III} and Cr^{III} may also take place (see below).

To our knowledge, there is no quantum theory for the magnetism of chains involving alternating A−B magnetic ions. However (see Supporting Information), the behavior of the infinite chain can be extrapolated by the exact results obtained for finite cyclic complexes $(Ni-Cr)_n$ when their size is increased (n). The χT versus T ($T > 15$ K) experimental data for **KCr** could be well simulated, using the program MAGPACK,[77−79] with oligomers of moderate size ($n = 5$), leading to J(NiCr) ($H_{exc} = -JS_1S_2$) values of 14.6 cm^{-1} and $g_{eff} = 2.15$ (see Figure 9a). It is worth mentioning that an alternative simulation using the theory of a classical alternating-spin Heisenberg[80] leads to a smaller value of J ($T > 14$ K, $g_{Ni} = 2.30$, $g_{Cr} = 1.99$, J(Ni−Cr) = 10.7 cm^{-1}, see Supporting Information).

The simple description in terms of a Heisenberg Hamiltonian breaks down for transition metal ions with orbitally degenerate ground states. The $^2T_2$ (t_{2g}^5) ground state of $[Fe(CN)_6]^{3-}$ is, in principle, Jahn−Teller unstable. Experimental and theoretical studies show, however, that Jahn−Teller instabilities in cyanide complexes with T ground states are very weak. Indeed, it was possible to simulate the magnetic susceptibility of $[Fe(CN)_6]^{3-}$ ($^2T_{2g}$, t_{2g}^5) and $[Mn(CN)_6]^{3-}$($^3T_{1g}$, t_{2g}^4) using cubic symmetry.[68] Unlike $[Mn(CN)_6]^{3-}$, however, the χT value of $[Fe(CN)_6]^{3-}$ shows a weak dependence on temperature and could be modeled reasonably well, using an $s = 1/2$ pseudo-pin approach, with an effective g value of about 3.00 (see Figure 9b). With the same approach as was used for the Ni−Cr chains, the χT versus T curve could be fitted with g_{eff}(Fe) = 2.50 and J(NiFe) = 9 cm^{-1} (Figure 9c).[81] Exchange coupling constants for Ni−Cr and Ni−Fe cyanide-bridged coupling pairs with almost linear NiNCM (M = Cr^{3+}, Fe^3) geometries, as reported in $NiLML'(CN)_x$ (M = Cr^{3+}, Fe^{3+}; $x = 2, 3, 4$) compounds with polydentate amines L and L′ from literature are listed in Table 5. In agreement with the rather similar bridging geometries found in these compounds, J(Ni−M) values vary in the narrow range of 14.6−21.8 cm^{-1} (for Ni−Cr) and between 6.6 and 11.0 cm^{-1} for Ni−Fe, respectively, with a weak dependence on the bonding of Ni and M to the terminal ligands. In contrast, the zero-field splitting parameters, D, for Ni obtained from magnetic susceptibility data are rather sensitive to the Ni^{2+} coordination geometry and vary from positive values (2.4 cm^{-1},[55] close to the value of D reported here, 2.7 cm^{-1}) to negative values in Ni^{2+} octahedra with a stronger (weaker) axial (equatorial) ligand field.[15,18,81]

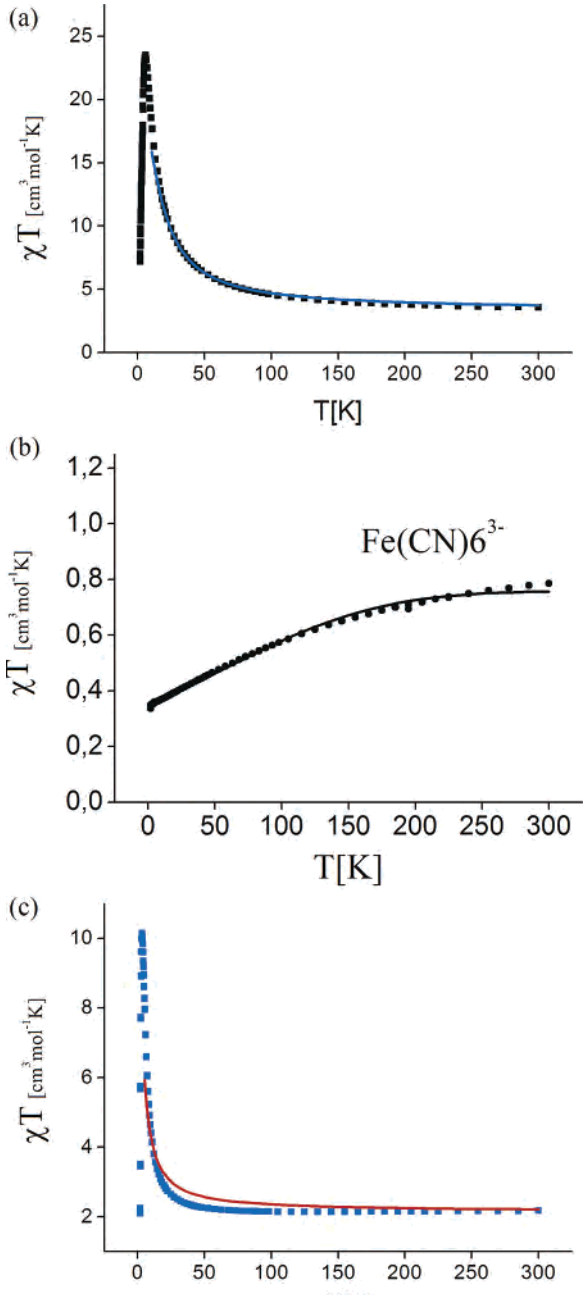

Figure 9. (a) Experimental (■, $B = 1$ kG) and simulated (—) χT vs T curves ($T > 14$ K) for **KCr**, using a cyclic $(NiCr)_5$ oligomer, J(NiCr) = 14.6 cm^{-1}, $g_{eff} = 2.15$ (MAGPACK). (b) Plot of χT vs T ($B = 1$ kG) of $Fe(CN)_6^{3-}$ in $[(Ph_3P)_2N]_3[Fe(CN)_6]\cdot xH_2O$; experimental and simulated data (adopting a cubic symmetry for $Fe(CN)_6^{3-}$[68]) are given by filled circles and a solid line, respectively. (c) Experimental (■, $B = 1$ kG) and simulated (—) χT vs T curves ($T > 14$ K) for **KFe** using a cyclic $(NiFe)_5$ cluster, J(NiFe) = 9.0 cm^{-1}, $g_{eff} = 2.50$ (MAGPACK).

(77) Borrás-Almenar, J. J.; Clemente-Juan, J. M.; Coronado, E.; Tsukerblat, B. MAGPACK, Magnetic Properties Analysis Package for Spin Clusters, version 00.1, 2000.
(78) Borrás-Almenar, J. J.; Clemente-Juan, J. M.; Coronado, E.; Tsukerblat, B. *Inorg. Chem.* **1999**, *38*, 6081.
(79) Borrás-Almenar, J. J.; Clemente-Juan, J. M.; Coronado, E.; Tsukerblat, B. *J. Comput. Chem.* **2001**, *9*, 985.
(80) Drillon, M.; Coronado, E.; Beltran, D.; Georges, R. *Chem. Phys.* **1983**, *79*, 449.
(81) These values can be compared with the (J, g_{eff}) set which is obtained when a chain of alternating $S = 1$ (Ni^{II}) and 1/2 (Fe^{III}) spins is used in a classical approximation ($J = 6.4$ cm^{-1}, 2.74) or with those obtained from a treatment in which the $S = 1/2$ spins have been accounted for quantum mechanically, while the $S = 1$ spin has been treated classically ($J = 13.5$ cm^{-1}, 2.70), see Supporting Information.

Table 5. Ni−N_{CN} and Cr−C_{CN}, as well as Fe−C_{CN} Bond Lengths (in Å) and *J* Parameters (in cm^{-1}), for Ni−NC−Cr and Ni−NC−Fe Exchange Coupling in NiLCrL′$(CN)_x$ and NiLFeL′$(CN)_x$ (L, L′ = amine ligands; $x = 2, 3, 4$) Compounds Obtained from a Fit to Magnetic Data[a]

magnetic core	*R*(Cr−C_{CN})	*R*(Ni−N_{CN})	*J*	dimensionality	ref
$CrNi_6$			16.8	0	40
Cr_8Ni_6	2.068	2.108	21.8	0	43
$CrNi_6$	2.077	2.113	17.3	0	49
$(CrNi)_n$	2.090	2.090	14.6	1	this work
Fe_4Ni_4	1.937	2.020	11.0	0	46
Fe_2Ni_3	1.918	2.055	8.6	0	47
Fe_2Ni_3	1.938	2.055	6.6	0	47
Fe_2Ni_3	1.937	2.045	10.7	0	55
Fe_2Ni_2	1.928	2.039	10.6	0	61
Fe_4Ni_4	1.926	2.060	12.7	0	65
$(FeNi)_n$	1.936	2.110	9.0	1	this work

[a] Average values for bond length differences.

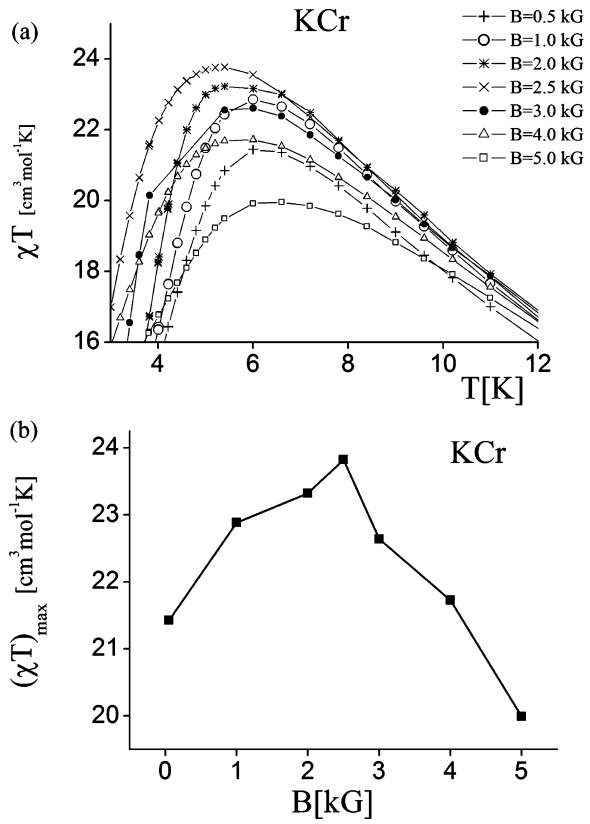

Figure 10. (a) Field dependence of the χT vs *T* behavior of **KCr** and (b) dependence of the maxima of the χT vs *T* curves for **KCr** from the applied magnetic field *B*.

So far, we have neglected interchain antiferromagnetic coupling. According to the structural data this can be mediated by M−CN−A−NC−M and M−CN−A−macrocycle−Ni contacts (M = Cr, Fe; see Figure 4b), and this might contribute to the low-temperature magnetic behavior, in addition to the Ni^{II} anisotropy. The sigmoidal shape of the magnetization versus field curves in Figure 8 (inset for **KCr**) is a typical pattern for metamagnets.[82] Apparently, there are important contributions from antiferromagnetic interactions between the chains to decrease χT when the temperature is reduced (see Figure 7).

(82) Carlin, R. L. *Magnetochemistry;* Springer-Verlag: Berlin, 1986.

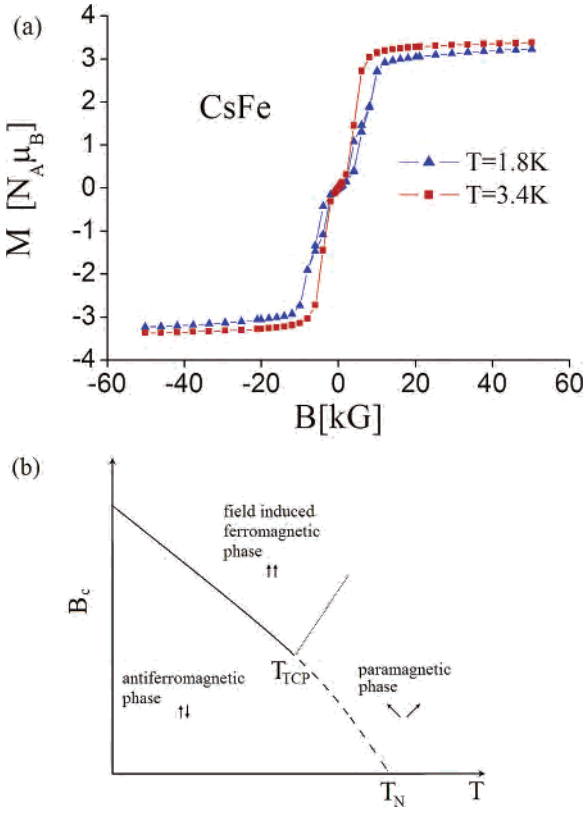

Figure 11. Hysteresis loops for **CsFe** at two different temperatures (a) and the phase diagram (schematic) of a metamagnet (b).

To check this hypothesis, the field dependencies of the magnetization have been measured in the narrow temperature range between 1.8 and 20 K. The results presented as χT versus *T* curves for **KCr** are shown in Figure 10a. It is remarkable that, upon increasing the magnetic field, *B*, from $B = 0.5$ kG, the maxima in χT move to higher values and reach a maximum value at $B = 2.5$ kG, after which they decrease with a further increase of the field. This is shown in Figure 10b. If we assume that the weak magnetic field affects only the weak interchain coupling and does not alter the ordering of spin states of Ni^{II} with $M_s = 0 \ll M_s = -1 < M_s = 1$, we can get specific information about the weak antiferromagnetic interactions between the chains. The increase of $(\chi T)_{max}$ up to the critical value of $B = 2.5$ kG suggests field-induced transitions from an antiferromagnetic to a ferromagnetic ground state. Such metamagnetic behavior is a well-known phenomenon in chain magnetism.[35,83] Our studies have shown that it is much more pronounced for the Fe^{III}-based chains than it is for the Cr^{III}-based chains, presumably because of the unquenched orbital momenta, which lead to an enhanced magnetic anisotropy.

Antiferromagnetic to ferromagnetic transitions for a critical magnetic field, B_c, are nicely demonstrated by the hysteresis loops for **CsFe**, which we used as an example (see Figure 11a). As shown by the typical phase diagram of a metamagnet (see Figure 11b), the B_c versus *T* phase line separates the antiferromagnetic phase (below the curve) from the upper

(83) Lloret, F.; Ruiz, R.; Julve, M.; Faus, J.; Jourunaux, Y.; Castro, I.; Verdaguer, M. *Chem. Mater.* **1992**, *4*, 1150.

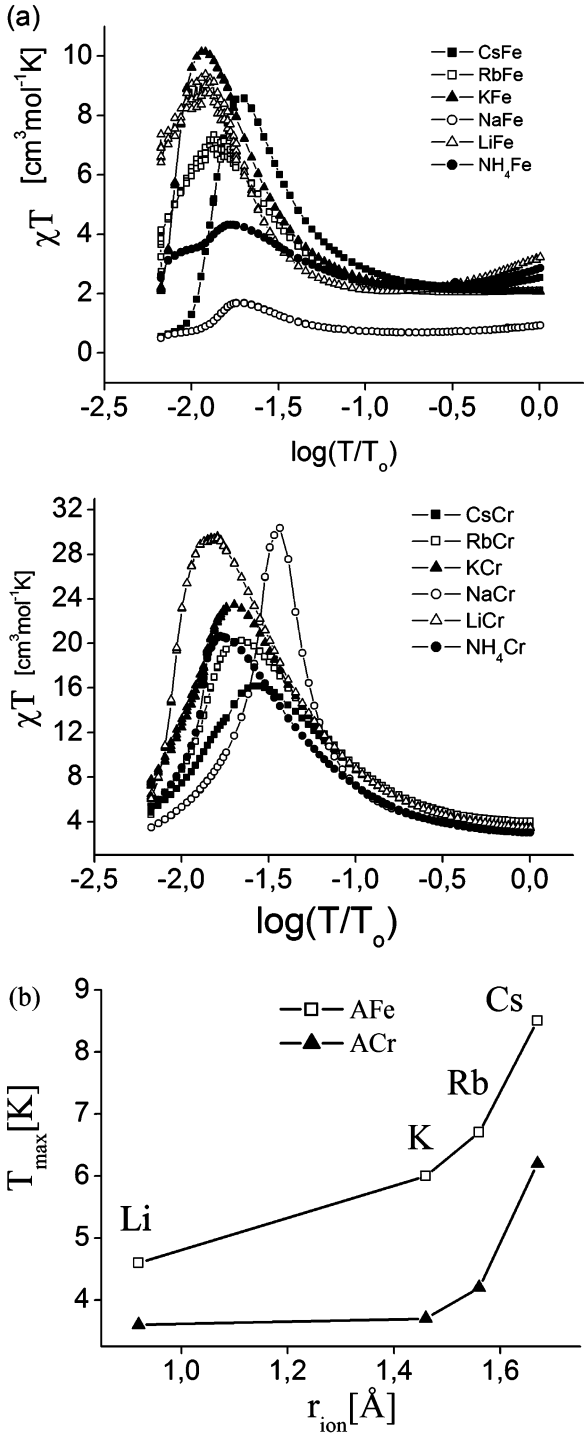

Figure 12. (a) χT vs T curves (B = 0.1 kG) for **AFe** (top) and **ACr** (bottom) (A = NH_4, Li, Na, K, Rb, and Cs), demonstrating the tuning of the magnetic properties by the singly charged counterion. (b) Values of $(T)_{max}$ from the curves in 12a vs the ionic radii of A; A = NH_4 is omitted because the interchain coupling is mediated by hydrogen bonding in this case. The curves for A = Na are omitted because of the poor crystallinity of the **NaM** samples (see Figure 1).

region, corresponding to domains where the field-induced ferromagnetic and paramagnetic phases found at lower- and higher-temperature regions, respectively can be stabilized. The two latter phases are well separated (dotted line in Figure 10b), but this is not easily accessible by experiment. At the three-critical point, T_{TCP}, the three phases coexist. For $T < T_{TCP}$, the antiferromagnetic-ferromagnetic transition is first order, and a hysteresis can be observed in the $M = f(B)$ curves, while for $T_{TCP} < T < T_N$, it is a second-order transition (dashed line in Figure 10b), and no hysteresis is present. The two curves $M = f(B)$ (Figure 10a) nicely manifest this for **CsFe** with a hysteretic behavior found for the lower (T = 1.8 K) but not the higher (T = 3.4 K) temperature measurement.

On the basis of the concept of weak interchain antiferromagnetic coupling, we have studied the effect of the counterion on the low-temperature magnetic behavior. In Figure 12a, we plot (χT) versus T curves for the **AFe** and **ACr** (A = NH_4, Li, Na, K, Rb, and Cs) series. As shown in Figure 12b, there is a clear correlation between the ionic radius of A and the value of T_{max}. If we take the latter value as a measure for the relative strength of interchain antiferromagnetic coupling (i.e., larger T_{max} results in stronger coupling), it follows that Cs is the best among the alkaline metal ions to mediate the coupling. Possibly, the hydrogen-bonding network, which could be the cause of the interchain interactions, is affected by the alkaline ions. Alternatively, a more active role of the alkaline metal ion in mediating exchange coupling than the purely electrostatic bonding implies could be made responsible for the counterion effect. A similar contribution of alkaline metal ions to the exchange has been observed in the electronic and magnetic properties of oxo-cuprates.[84]

Conclusions and Outlook

Magnetic susceptibility and magnetization data of a series of Ni^{II} **ACr**, **AFe**, and **ACo** complexes demonstrate new efficient pathways for ferromagnetic exchange interactions between Ni^{II} and Fe^{III} or Cr^{III}. These are stronger than those found in oligonuclear cyanometalates with Cu^{II} in a pseudo-square-planar configuration, which makes, because of the Jahn−Teller activity, more distant contacts to neighboring exchange-coupled Fe^{III} and Cr^{III} magnetic centers and weakens the exchange coupling. We have demonstrated, with simulations of the susceptibility curves, that Ni−Cr ferromagnetic coupling is stronger than Ni−Fe coupling.

One additional feature which emerges from our analysis, based on the optical spectra, is the single-ion Ni(II) anisotropy in *trans*-Ni(ammine)$_4$(NC)$_2$, which significantly affects the low-temperature magnetic behavior. Such influences are frequently ignored. Field dependencies of the magnetization at low temperatures and low magnetic field indicate a weak interchain antiferromagnetic coupling, which can be switched to ferromagnetic interactions upon an increase in the magnetic field (metamagnetic behavior). Along the same lines, it has been found that the interchain magnetic coupling can be tuned by changing the alkaline counterions, and synthetic strategies for this have been developed.

Experimental Section

Measurements. Infrared spectra (KBr pellets) were recorded with a Perkin-Elmer 16 PC FT-IR spectrophotometer. UV−vis spectra were measured on a Jasco V-570 UV/VIS/NIR instrument

(84) Geertsma, W.; Khomskii, D. *Phys. Rev. B*, **1996**, *54*, 3011.

(diffuse reflectance, polytetrafluoroetylene pellets). X-ray powder diffraction experiments were performed using a Philips XPert diffractometer with Cu Kα radiation and a secondary beam monochromator. The scan rate was 0.008°/s. Samples were mortared under ethanol and spread onto glass slides. Magnetic measurements were performed in "zero-field " and "field-cooling" modes (DC) using a Quantum Design MPMS XL magnetometer equipped with a 50 kG magnet, operating in the temperature range of 300−1.8 K. Powdered samples were maintained in gelatin containers, and the data were corrected for the diamagnetism of the container; Pascal's constants were used for diamagnetic correction of the samples.

Interpretation of the Magnetic Data. The electronic absorption spectra of the $[Ni(NHR_2)_4(NC)_2]^{2+}$ chromophore were interpreted with the aid of the AOMX program.[85,86]

The magnetic data were simulated using the program MAGPACK[77] and, independently, by our own programs which gave identical results for smaller cyclic magnetic complexes. Larger oligomers were simulated with MAGPACK, and convergence of the χT values was achieved (for $T > 15$) with five (Ni−M) (M = Cr,Fe) units (Supporting Information). Independently, a classical model of a magnetic chain with alternating $S = 1$ (Ni^{2+}) and 3/2 (Cr^{3+}) or 1/2 (Fe^{3+}) magnetic ions[80] and, alternatively, for **KFe**, a coupled classical-spin (Ni^{2+}, S = 1) quantum-spin (Fe^{3+}, S = 1/2) alternating Ni−Fe chain were used to simulate the χT versus T behavior (see Supporting Information). A nonlinear optimization procedure has been adopted to yield Ni−Cr (for **KCr**) and Ni−Fe (for **KFe**) exchange-coupling constants from the experimental magnetic susceptibilities in the latter two cases.

Crystal Structure Determinations. Crystal and intensity data were obtained at low temperature with a STOE IPDS (complex **KFe**) and a Bruker AXS Smart 1000 CCD diffractometer (Mo Kα radiation, Table 6). Analytical (complex **KFe**) or semiempirical absorption corrections were applied. The crystals of complex **LiCr** were found to be racemically twinned. The structures were solved by heavy atom or direct methods and refined by full-matrix least squares based on F^2 using all measured unique reflections. All non-hydrogen atoms, except for some of the oxygen atoms of the fractionally populated water molecules, were given anisotropic displacement parameters. Most of the hydrogen atoms were input in calculated positions. In most of the structures, the amine hydrogen atoms of the pentaazacyclotetradecane macrocycle were located in difference Fourier syntheses and refined with the N−H distances restrained to be equal. The calculations were performed using the programs DIRDIF,[87] SIR2002,[88] SHELXS-86,[89] SHELXL-97,[90] and PLATON.[91]

Materials. $K_3[Cr(CN)_6]$, $K_3[Fe(CN)_6]$, $K_3[Co(CN)_6]$, $LiNO_3$, $NaNO_3$, KNO_3, RbCl, CsCl, and NH_4NO_3 were purchased from Aldrich or Fluka and used without purification; $[NiL](ClO_4)_2 \cdot H_2O$[72] (**1**) was obtained as described previously.

Syntheses. Several synthetic procedures were developed to obtain solids of good crystallinity (i.e., crystals of X-ray quality, if possible). The effectiveness of different procedures depends on the nature of the simply charged cation involved. Procedures 1−3 differ with respect to the concentration of the starting compounds in the initial solutions. In the reports below, the yield of products was ∼80% each, with respect to complex **1**.

Procedure 1. A solution of **1** (10 mL, 17.1 mmol·L^{-1}) was added to a solution of the potassium salt of the corresponding hexacyanometalate (10 mL, 171 mmol L^{-1}). The initially formed precipitate was dissolved upon the addition of excess cyanometalate, and the clear reaction mixture was added to a solution of the nitrate salt of the singly charged cation (30 mL, 8 mol L^{-1}). The vessel was left undisturbed overnight (sometimes longer) until nicely shaped crystals were formed. The product was washed with water by decantation to remove some amorphous precipitate, filtered off, washed with water and ethanol, and dried in air.

Li[NiL][Fe(CN)$_6$]·5H$_2$O (LiFe). Anal. Calcd for $C_{18}H_{36}N_{16}O_5NiFeLi$ (678.06): C, 31.88; H, 5.35; N. 33.05. Found: C, 31.73; H, 5.25; N, 33.08. IR (KBr): ν(CN) 2146, 2116.

Li[NiL][Co(CN)$_6$]·5H$_2$O (LiCo). Anal. Calcd for $C_{18}H_{36}N_{16}O_5NiCoLi$ (681.15): C, 31.74; H, 5.33; N, 32.90. Found: C, 31.71; H, 5.44; N, 32.64. IR (KBr): ν(CN) 2162, 2128.

Na[NiL][Fe(CN)$_6$]·4H$_2$O (NaFe). Anal. Calcd for $C_{18}H_{34}N_{16}O_4NiFeNa$ (676.10): C, 31.98; H, 5.07; N, 33.15. Found: C, 32.47; H, 5.39; N, 33.21. IR (KBr): ν(CN) 2155, 2136, 2112.

Na[NiL][Cr(CN)$_6$]·5H$_2$O (NaCr). Anal. Calcd for $C_{18}H_{36}N_{16}O_5NiCrNa$ (690.26): C, 31.32; H, 5.26; N, 32.48. Found: C, 31.68; H, 6.06; N, 32.79. IR (KBr): ν(CN) 2150, 2128.

Na[NiL][Co(CN)$_6$]·4H$_2$O (NaCo). Anal. Calcd for $C_{18}H_{34}N_{16}O_4NiCoNa$ (679.18): C, 31.83; H, 5.05; N, 33.00. Found: C, 32.14; H, 5.31; N, 32.83. IR (KBr): ν(CN) 2149, 2127.

K[NiL][Fe(CN)$_6$]·3H$_2$O (KFe). Anal. Calcd for $C_{18}H_{32}N_{16}O_3NiFeK$ (674.19): C, 32.07; H, 4.78; N, 33.24. Found: C, 31.70; H, 4.68; N, 33.19. IR (KBr): ν(CN) 2156, 2136, 2112.

K[NiL][Cr(CN)$_6$]·3H$_2$O (KCr). Anal. Calcd for $C_{18}H_{32}N_{16}O_3NiCrK$ (670.34): C, 32.25; H, 4.81; N, 33.43. Found: C, 32.14; H, 4.90; N, 33.17. IR (KBr): ν(CN) 2148, 2160, 2124.

NH$_4$[NiL][Fe(CN)$_6$]·3H$_2$O (NH$_4$Fe). Anal. Calcd for $C_{18}H_{36}N_{17}O_3NiFe$ (653.13): C, 33.10; H, 5.56; N, 36.46. Found: C, 33.22; H, 5.50; N, 35.48. IR (KBr): ν(CN) 2155, 2136, 2116.

NH$_4$[NiL][Co(CN)$_6$]·3H$_2$O (NH$_4$Co). Anal. Calcd for $C_{18}H_{36}N_{17}O_3NiCo$ (656.22): C, 32.95; H, 5.53; N, 36.29. Found: C, 32.64; H, 5.62; N, 35.75. IR (KBr): ν(CN) 2172, 2152, 2123.

Procedure 2. A solution of **1** (10 mL, 8.6 mmo ·L^{-1}) was added to solution of the potassium salt of the corresponding hexacyanometalate (10 mL, 171 mmol L^{-1}). This solution was added to a solution of the nitrate salt of singly charged cation (30 mL, 8 mol L^{-1}). The product was collected as described in Procedure 1 above.

K[NiL][Co(CN)$_6$]·4H$_2$O (KCo). Anal. Calcd for $C_{18}H_{34}N_{16}O_4NiCoK$ (695.29): C, 31.09; H, 4.93; N, 32.23. Found: C, 31.53; H, 4.79; N, 32.26. IR (KBr): ν(CN) 2172, 2150, 2125.

NH$_4$[NiL][Cr(CN)$_6$]·3H$_2$O (NH$_4$Cr). Anal. Calcd for $C_{18}H_{36}N_{17}O_3NiCr$ (649.28): C, 33.30; H, 5.59; N, 36.67. Found: C, 33.38; H, 5.60; N, 35.46. IR (KBr): ν(CN) 2160, 2148, 2128.

Procedure 3. A solution of **1** (10 mL, 4.3 mmol L^{-1}) was added to a solution of $K_3[Cr(CN)_6]$ (10 mL, 171 mmol L^{-1}). This solution was added to a solution of $LiNO_3$ (30 mL, 8 mol L^{-1}). The product was collected as described in Procedure 1 above.

(85) Adamsky, H. AOMX, a FORTRAN program for calculation of dn electron terms in the framework of angular overlap model, http:/www.aomx.de.

(86) Adamsky, H.; Atanasov, M.; Schönherr, *T.AOMX: Angular Overlap Model Computation, Comprehensive Coordination Chemistry II, From Biology to Nanotechnology, Volume I: Fundamentals*; Lever, A. B. P., Ed.; Elsevier: New York, 2003; Vol. 2, Section 2.52, p 661.

(87) Beurskens, P. T.; Beurskens, G.; de Gelder, R.; Ganda, S. G.; Gould, R. O.; Israel, R.; Smits, J. M. M. *DIRDIF-99*; University of Nijmegen: Nijmegen, The Netherlands, 1999.

(88) Burla, M. C.; Camalli, M.; Carrozzini, B.; Cascarano, G. L.; Giacovazzo, C.; Polidori, G.; Spagna, R. *SIR2002*; University of Bari: Bari, Italy, 2002.

(89) Sheldrick, G. M. *SHELXS-86*; University of Göttingen: Göttingen, Germany, 1986.

(90) Sheldrick, G. M. *SHELXS-97, Program for structure solution*; *SHELXL-97 Program for structure refinement*; University of Göttingen: Göttingen, Germany, 1997.

(91) Spek, A. L. *J. Appl. Crystallogr.* **2003**, *36*, 7.

Table 6. Crystal Data and Structure Refinement

	KFe	RbFe	CsFe
empirical formula	$C_{36}H_{44}Fe_2K_2N_{32}Ni_2Rb_2 \cdot 8H_2O$	$C_{36}H_{52}Fe_2N_{32}Ni_2Rb_2 \cdot 7H_2O$	$C_{36}H_{52}Cs_2Fe_2N_{32}Ni_2 \cdot 7H_2O$
fw	688.24	1459.27	1554.15
temp (K)	200(2)	100(2)	100(2)
cryst syst	orthorhombic	orthorhombic	orthorhombic
space group	*Pbca*	*Pbca*	*Pbca*
unit cell dimensions (Å)			
a	24.410(2)	24.2333(13)	24.4696(11)
b	11.528(1)	11.6957(6)	11.7515(6)
c	41.176(3)	41.013(2)	41.0003(19)
vol (Å^3)	11 587(2)	11 624.2(11)	11 789.8(10)
Z	8	8	8
density (calcd) (Mg m^{-3})	1.578	1.668	1.751
abs coeff (mm^{-1})	1.350	2.865	2.401
F_{000}	5680	5952	6240
cryst size (mm^3)	0.30 × 0.14 × 0.04	0.17 × 0.15 × 0.10	0.25 × 0.25 × 0.17
θ range (deg)	1.67−24.06	0.99−25.35	0.99−26.00
index ranges (*h*, *k*, *l*)	−25−27, −13−12, −4−47	0−29, 0−14, 0−49	0−30, 0−14, 0−50
reflns collected	38 451	133 992	130 754
independent reflns	9068 [R_{int} = 0.1152]	10 642 [R_{int} = 0.1017]	11 603 [R_{int} = 0.1509]
completeness (%) [θ (deg)]	99.0 [24.06]	100.0 [25.35]	100.0 [26.00]
max and min transm	0.9373 and 0.6648	0.7626 and 0.6340	0.6786 and 0.5851
data/restraints/params	9068/0/739	10 642/28/755	11 603/0/731
GOF on F^2	0.770	1.078	1.078
Final R indices [$I > 2\sigma(I)$]	R1 = 0.0554, wR2 = 0.1037	R1 = 0.0561, wR2 = 0.1419	R1 = 0.0740, wR2 = 0.1761
R indices (all data)	R1 = 0.1300, wR2 = 0.1209	R1 = 0.0840, wR2 = 0.1548	R1 = 0.1277, wR2 = 0.2034
RMS residual density,	0.097,	0.140,	0.259,
largest diff peak and hole (e Å^{-3})	0.706 and −0.647	1.216 and −1.916	2.113 and −1.652

	NH_4Cr	LiCr	KCr
empirical formula	$C_{36}H_{52}Cr_2N_{34}Ni_2 \cdot 5.9\ H_2O$	$C_{18}H_{26}CrLiN_{16}Ni \cdot 5\ H_2O$	$C_{36}H_{52}Cr_2K_2N_{32}Ni_2 \cdot 7.4\ H_2O$
fw	1296.44	674.28	1358.76
temp (K)	100(2)	100(2)	100(2) K
cryst syst	orthorhombic		
space group	*Pbca*	*Pca*2$_1$	*Pbca*
unit cell dimensions (Å)	*a* = 24.3293(13)	*a* = 25.3210(12)	*a* = 24.3293(13)
a	*b* = 11.6824(6)	*b* = 10.5408(5)	*b* = 11.6824(6)
b	*c* = 41.935(2)	*c* = 11.8223(5)	*c* = 41.935(2)
c	11919.0(11)	3155.4(3)	11919.0(11)
vol (Å^3)	8	4	8
Z	1.445	1.419	1.514
density (calcd) (Mg m^{-3})	1.048	0.996	1.189
abs coeff (mm^{-1})	5414	1404	5600
F_{000}	0.25 · 0.20 · 0.20	0.25 · 0.15 · 0.15	0.17 · 0.15 · 0.10
cryst size (mm^3)	0.97 to 25.03	1.61 to 30.03	0.97 to 25.07
θ range (deg)	0...28, 0...13, 0...49	0...35, 0...14, −16...16	0...28, 0...13, 0...50
index ranges (*h*, *k*, *l*)	70508	27056	131883
reflns collected	10519 [R_{int} = 0.0743]	8590 [R_{int} = 0.0449]	10415 [R_{int} = 0.1226]
independent reflns	100.0 [25.03]	100.0 [30.03]	98.6 [25.07]
completeness (%) [θ (deg)]	0.8178 and 0.7796	0.8650 and 0.7888	0.8903 and 0.8189
max and min transm	10519/28/747	8590/7/393	10415/28/775
data/restraints/params	1.091	1.048	1.097
GOF on F^2	*R*1 = 0.0550, w*R*2 = 0.1554	*R*1 = 0.0439, w*R*2 = 0.1130	*R*1 = 0.0651, w*R*2 = 0.1654
Final R indices [$I > 2\sigma(I)$]	*R*1 = 0.0891, w*R*2 = 0.1675	*R*1 = 0.0650, w*R*2 = 0.1232	*R*1 = 0.1027, w*R*2 = 0.1821
R indices (all data)	0.099, 1.310 and −0.732	0.086, 1.075 and −0.350	0.121, 0.892 and −2.050

Li[NiL][Cr(CN)$_6$]·5H$_2$O (LiCr). Anal. Calcd for $C_{18}H_{36}N_{16}O_5NiCrLi$ (674.21): C, 32.07; H, 5.38; N, 33.24. Found: C, 32.63; H, 5.27; N, 33.51. IR (KBr): ν(CN) 2153, 2146, 2128.

Procedure 4. A solution of **1** (1 mL, 17.1 mmol L^{-1}) was added to a solution of the potassium salt of the corresponding hexacyanometalate (1 mL, 171 mmol L^{-1}). This solution was layered over a solution of RbCl or CsCl (3 mL, 8 mol L^{-1}). Diffusion was complete in several days, and the product was collected as described in Procedure 1 above.

Rb[NiL][Fe(CN)$_6$]·4H$_2$O (RbFe). Anal. Calcd for $C_{18}H_{34}N_{16}O_4NiFeRb$ (738.57): C, 29.22; H, 4.64; N, 30.34. Found: C, 29.79; H, 4.57; N, 30.25. IR (KBr): ν(CN) 2155, 2137, 2112.

Rb[NiL][Cr(CN)$_6$]·3H$_2$O (RbCr). Anal. Calcd for $C_{18}H_{32}N_{16}O_3NiCrRb$ (716.71): C, 30.16; H, 4.50; N, 31.27. Found: C, 30.01; H, 4.37; N, 31.33. IR (KBr): ν(CN) 2160, 2151, 2126.

Rb[NiL][Co(CN)$_6$]·3H$_2$O (RbCo). Anal. Calcd for $C_{18}H_{32}N_{16}O_3NiCoRb$ (723.65): C, 29.88; H, 4.46; N, 30.97. Found: C, 29.61; H, 4.30; N, 30.82. IR (KBr): ν(CN) 2171, 2150, 2124.

Cs[NiL][Fe(CN)$_6$]·3H$_2$O (CsFe). Anal. Calcd for $C_{18}H_{32}N_{16}O_3NiFeCs$ (768.00): C, 28.15; H, 4.20; N, 29.18. Found: C, 28.65; H, 4.27; N, 28.98. IR (KBr): ν(CN) 2155, 2138, 2112.

Cs[NiL][Cr(CN)$_6$]·2H$_2$O (CsCr). Anal. Calcd for $C_{18}H_{30}N_{16}O_2NiCrCs$ (746.13): C, 28.98; H, 4.05; N, 30.04. Found: C, 29.22; H, 4.21; N, 29.90. IR (KBr): ν(CN) 2162, 2151, 2126.

Cs[NiL][Co(CN)$_6$]·2H$_2$O (CsCo). Anal. Calcd for $C_{18}H_{30}N_{16}O_2NiCoCs$ (753.07): C, 28.71; H, 4.02; N, 29.76. Found: C, 28.85; H, 4.35; N, 29.52. IR (KBr): ν(CN) 2151, 2124.

Acknowledgment. Financial support by the German Science Foundation (DFG) is gratefully acknowledged. We thank Christoph Busche for remeasuring the low-temperature magnetic data and Gopalan Rajaraman for help with MAGPACK.

Supporting Information Available: Figure showing the IR spectrum of **KFe**, tables showing the maxima of the CN vibrations

in the IR spectrum and bond lengths and angles for the complexes, and the theory and implementation for the magnetism determination. This material is available free of charge via the Internet at http://pubs.acs.org. Crystallographic data (excluding structure factors) for the structures reported in this paper have been deposited with the Cambridge Crystallographic Data Centre as supplementary publications. Copies of the data can be obtained free of charge upon application to CCDC, 12 Union Road, Cambridge CB2 1EZ, UK (fax +(44) 1223-336-033; e-mail deposit@ccdc.cam.ac.uk).

IC060453Q